ACS OMEGA

Article

Cite This: ACS Omega 2018, 3, 14538−14550

http://pubs.acs.org/journal/acsodf

"Weakly Ligated, Labile Ligand" Nanoparticles: The Case of $Ir(0)_n{\cdot}(H^+Cl^-)_m$

Joseph E. Mondloch,[†] Saim Özkar,[‡] and Richard G. Finke*[,†]

[†]Department of Chemistry, Colorado State University, Fort Collins, Colorado 80523, United States

[‡]Department of Chemistry, Middle East Technical University, 06800 Ankara, Turkey

Supporting Information

ABSTRACT: It is of considerable interest to prepare weakly ligated, labile ligand (WLLL) nanoparticles for applications in areas such as chemical catalysis. WLLL nanoparticles can be defined as nanoparticles with sufficient, albeit minimal, surface ligands of moderate binding strength to meta-stabilize nanoparticles, initial stabilizer ligands that can be readily replaced by other, desired, more strongly coordinating ligands and removed completely when desired. Herein, we describe WLLL nanoparticles prepared from $[Ir(1,5\text{-COD})Cl]_2$ reduction under H_2, in acetone. The results suggest that H^+Cl^--stabilized $Ir(0)_n$ nanoparticles, herein $Ir(0)_n{\cdot}(H^+Cl^-)_a$, serve as a WLLL nanoparticle for the preparation of, as illustrative examples, five specific nanoparticle products: $Ir(0)_n{\cdot}(Cl^-Bu_3NH^+)_a$, $Ir(0)_n{\cdot}(Cl^-Dodec_3NH^+)_a$, $Ir(0)_n{\cdot}(POct_3)_{0.2n}(Cl^-H^+)_b$, $Ir(0)_n{\cdot}(POct_3)_{0.2n}$, and the γ-Al_2O_3-supported heterogeneous catalyst, $Ir(0)_n{\cdot}(\gamma\text{-}Al_2O_3)_a(Cl^-H^+)_b$. (where a and b vary for the differently ligated nanoparticles; in addition, solvent can be present as a nanoparticle surface ligand). With added $POct_3$ as a key, prototype example, an important feature is that a minimum, desired, experimentally determinable amount of ligand (e.g., just 0.2 equiv $POct_3$ per mole of Ir) can be added, which is shown to provide sufficient stabilization that the resultant $Ir(0)_n{\cdot}(POct_3)_{0.2n}(Cl^-H^+)_b$ is isolable. Additionally, the initial labile ligand stabilizer HCl can be removed to yield $Ir(0)_n{\cdot}(POct_3)_{0.2n}$ that is >99% free of Cl^- by a AgCl precipitation test. The results provide strong support for the weakly ligated, labile ligand nanoparticle concept and specific support for $Ir(0)_n{\cdot}(H^+Cl^-)_a$ as a WLLL nanoparticle.

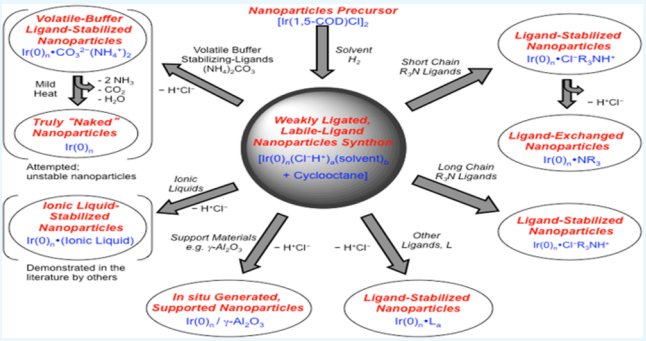

INTRODUCTION

Transition-metal nanoparticles are of significant interest within the catalysis community.[1−5] Because bulk metal is thermodynamically favored compared to metal(0) nanoparticles, stabilizing ligands are needed to prevent agglomeration of the resultant nanoparticles in solution.[6] Unfortunately, many (albeit not all[7]) common stabilizers bind strong enough to nanoparticle catalyst surfaces to act as catalyst poisons.[8,9] This includes many of the ligands that have led to what are otherwise valuable advances in the synthesis of size- and shape-controlled transition-metal nanoparticles.[10−15]

There have been many attempts to remove nanoparticle surface ligands, including extensive treatments such as thermal activation in N_2, H_2, and O_2 environments,[16−20] UV/ozone,[21−25] O_2/plasma,[24] and neutron sputtering.[26] Complete (100%) removal of nanoparticle-stabilizing ligands and polymers without inducing nanoparticle agglomeration or oxidizing the nanoparticle surface has proven largely unsuccessful, not unexpectedly.[17−21,23,24] A related problem of current interest is establishing and controlling a precise nanoparticle surface composition,[27] ill-defined and uncontrolled nanoparticle composition in turn affecting key catalytic properties such as catalytic selectivity, activity, lifetime, recovery, and recyclability.[28]

There have also been a number of reports attempting to prepare putatively "naked" nanoparticles that, in at least the literal interpretation of naked, would be devoid of any ligands, even solvent.[8,29−34] Although there have been claims of naked nanoparticles in the literature,[35−37] nanoparticle surfaces will of course never be truly naked in solution because even solvent-to-metal bond energies are 10 ± 3 kcal/mol for even the extreme case of metal−alkane bonds, at least in small-molecule organometallic complexes.[38−41] Solvent-only stabilized nanoparticles have been claimed in the literature,[42−46] but often anionic ligands (such as Cl^-, OAc^-, or other anions present in the synthetic precursor) are present but have not been tested, nor hence ruled out, as actual sources of nanoparticle stabilization. For example, in a recent report,[35] Pt(0) nanoparticles generated in acetic acid are claimed to be naked, but the high probability of surface OAc^- as a stabilizing ligand was not tested nor ruled out. We discuss putatively

Received: July 7, 2018
Accepted: September 27, 2018
Published: November 1, 2018

naked nanoparticles more in the Supporting Information (SI) for the interested reader.

Scheme 1. Nanoparticle Formation Stoichiometry and Acetone Hydrogenation Activity of $Ir(0)_n{\cdot}(Cl^-H^+)_a(acetone)_b$ WLLL Nanoparticles Starting from $[Ir(1,5\text{-}COD)Cl]_2$ in Neat Acetone at 22 °C under an Initial 3.7 atm of H_2[59]

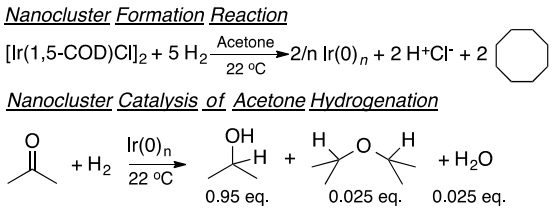

Hence, an unrealized goal is to prepare nanoparticles that have only relatively weakly bound, kinetically labile ligands, which provide a near-minimum level of nanoparticle meta-stabilization, which we have termed "weakly ligated, labile ligand" (WLLL) nanoparticles.[6,38,47] Such nanoparticles could, then and in principle, serve as a key synthetic structural unit/building block—that is, as a (nanoparticle) synthon—for use in the preparation of differently ligated nanoparticles and other nanoparticle products, the word synthon having been coined by Corey in 1967.[48] Such nanoparticles would then have a relatively precise, well-defined set of (at least average) ligands, plus any bound solvent, for applications in catalysts and other areas. It would be valuable synthetically to be able to add pretty much any desired ligand to a nanoparticle synthon, especially if sub-stoichiometric amounts (ligand/metal $\ll 1$) could be used thereby leaving surface sites available—that is, providing coordinative unsaturation—for catalysis or other applications and also opening up the use of the ligand/metal ratio for nanoparticle size and catalytic activity control.[49−52]

Worth noting here is that minimally stabilized, meta-stable, substitutionally labile metal complexes that are (or behave as if they are) coordinatively unsaturated are an important concept in classical organometallic chemistry. Notable here are complexes such as Wilke's classic "naked nickel", $Ni^0(1,5\text{-}COD)_2$,[53] $M(1,5\text{-}COD)_2^{n+}$ or $(M(1,5\text{-}COD)Cl_x)_y$ (M = Ir, Rh, Pt, Ru),[54,55] $M(NCCH_3)_x^{n+}(BF_4)_n$ complexes ($M = Mn^{II}$, Fe^{II}, Co^{II}, Cu^{II}, Cu^{I}, Zn^{II}),[56] as well as other examples one can find in the literature.[57,58] Indeed, $Ir(1,5\text{-}COD)Cl_2$ is a key starting material in the present contribution. It follows that development of lightly stabilized, meta-stable, effectively coordinatively unsaturated, WLLL nanoparticles can be expected to have an analogous, sizable, positive impact on nanoparticle science.

We previously reported that Ir(0) nanoparticles obtained from H_2 reduction of $[Ir(1,5\text{-}COD)Cl]_2$ in acetone are formed according to the balanced reaction in Scheme 1.[59] By design, this simple, clean reaction produces Ir(0) nanoparticles[59,60] that have only two possibilities for surface ligands, H^+Cl^- and acetone solvent, that is, $Ir(0)_n{\cdot}(Cl^-H^+)_a(acetone)_b$—and as such, they are a prototype example of WLLL nanoparticles. The formation of discrete 1.8 ± 0.5 nm $Ir(0)_n$ nanoparticles is evident from transmission electron microscopy (TEM) imaging of a sample harvested at an early stage of the acetone

Scheme 2. Formation and Possible Applications of $Ir(0)_n{\cdot}(Cl^-H^+)_a(acetone)_b$ as a Weakly Ligated, Labile Ligand (WLLL) Precursor[a]

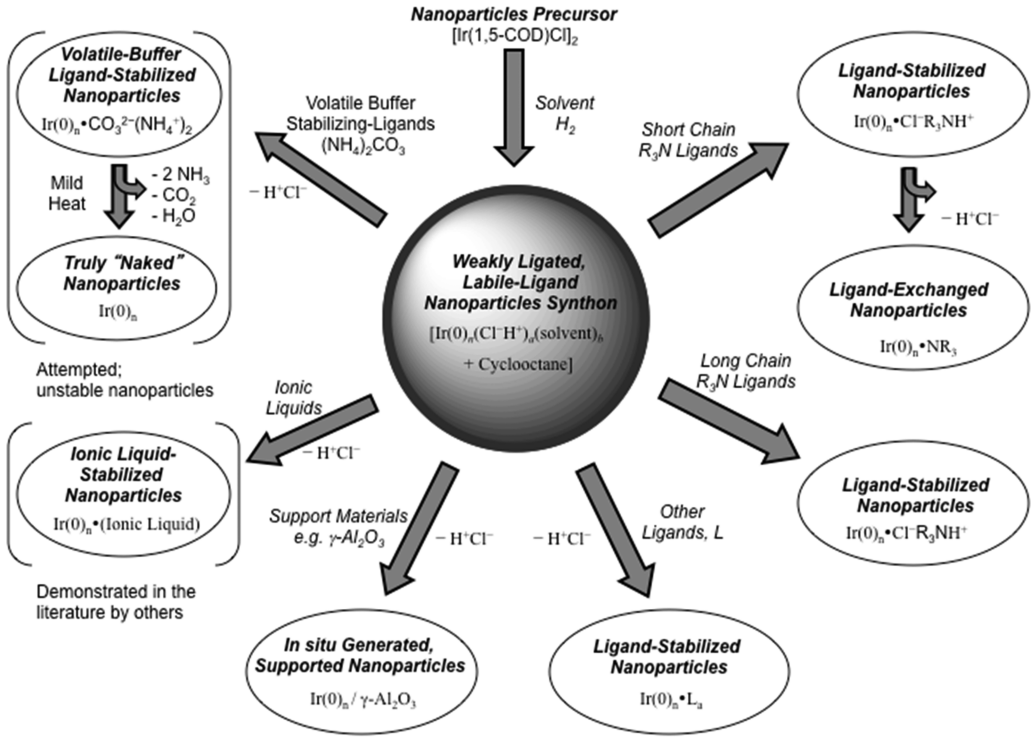

[a]The $Ir(0)_n{\cdot}(Cl^-H^+)_a(acetone)_b$ is shown as a true synthon in the scheme to illustrate the concept; it should be noted, however, that, in the present work, the $Ir(0)_n{\cdot}(Cl^-H^+)_a(acetone)_b$ is not premade or preisolated, but rather is formed in situ with the added ligands such as R_3N and $POct_3$, or solid support, $\gamma\text{-}Al_2O_3$.

DOI: 10.1021/acsomega.8b01569
ACS Omega 2018, 3, 14538−14550

hydrogenation reaction, as shown in Figure 1 of the original paper.[59]

Pleasingly, the $Ir(0)_n{\cdot}(Cl^-H^+)_a(acetone)_b$ nanoparticles proved to be an exceptionally active and selective acetone hydrogenation catalyst (1.9 turnovers/s at 22 °C to 95% 2-propanol; 16 400 total catalytic turnovers).[59] The acid-assisted catalytic hydrogenation of acetone was corroborated by the inhibition of catalysis (no catalytic turnover) if H^+ is scavenged from solution by using Proton Sponge (1,8-bis-(dimethylamino)naphthalene) as a strong, noncoordinating base[62] and by the unusual kinetics of the reaction that were, however, explicable in terms of the HCl requirement for acetone hydrogenation.[59]

The above results, while encouraging and quite supportive of the WLLL nanoparticle concept, left a number of additional, remaining possible uses of the WLLL $Ir(0)_n$ nanoparticles to be examined (Scheme 2). We note that others have already contributed to this scheme, notably the ionic liquid studies from Dupont's labs that will be referenced and detailed in a later section.

Herein, we report the additional studies probing the WLLL nanoparticle concept in the case of $Ir(0)_n{\cdot}(Cl^-H^+)_a(acetone)_b$ of: (i) adding Bu_3N to make $Ir(0)_n{\cdot}(Cl^-Bu_3NH^+)_b$ nanoparticles; (ii) subsequently removing H^+Cl^- to yield $Ir(0)_n{\cdot}(NBu_3)_c$ nanoparticles; (iii) adding longer-chain $Dodec_3N$ to yield $Ir(0)_n{\cdot}(Cl^-Dodec_3NH^+)_b$ nanoparticles; and importantly (iv) adding $POct_3$ and removing H^+Cl^- to yield $Ir(0)_n{\cdot}(POct_3)_d$ catalytically active nanoparticles, where the ratio of $POct_3$/Ir is small, 0.1−0.2. In addition, we report (v) adding γ-Al_2O_3 (and removing H^+Cl^-) to yield $Ir(0)_n{\cdot}\gamma$-Al_2O_3 catalytically active nanoparticles. The results suggest that $Ir(0)_n{\cdot}H^+Cl^-$ can serve as a WLLL en route to composition- and surface ligand-controlled nanoparticles for catalysis and other applications.

RESULTS AND DISCUSSION

$Bu_3NH^+Cl^-$-Stabilized Nanoparticles from $[Ir(1,5\text{-COD})Cl]_2$ Plus Bu_3N. Starting with $[Ir(1,5\text{-COD})Cl]_2$, $Bu_3NH^+Cl^-$-stabilized $Ir(0)_n{\cdot}(Cl^-Bu_3NH^+)_a$ nanoparticles were synthesized in acetone under H_2 and now in the presence of 1 equiv Bu_3N (Scheme 3).

Scheme 3. Stoichiometry of Formation of $Bu_3NH^+Cl^-$-Stabilized $Ir(0)_n$ Nanoparticles

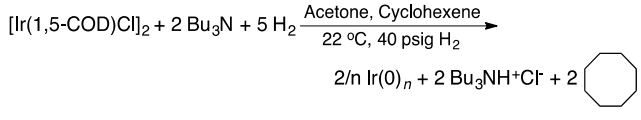

The stoichiometry of the reaction was confirmed via cyclooctane evolution, where 1.0 ± 0.1 equiv per mole of Ir were evolved. The reaction was monitored indirectly by having 1375 equiv of cyclohexene (vs Ir) present, that is, by our well-precedented method of a cyclohexene hydrogenation reporter reaction that reports the formation of catalytically active $Ir(0)_n$ nanoparticles (Figure 1).[59] Note that the evolution of 1.0 ± 0.1 equiv cyclooctane per Ir and no detectible amount of cyclohexene after hydrogenation (as determined by gas chromatography (GC) and NMR) indicate the complete conversion of cyclohexene to cyclohexane. Hence, no cyclohexene remains so that cyclohexene needs not be considered as a possible nanoparticle surface ligand. The resultant $Ir(0)_n{\cdot}Bu_4NH^+Cl^-$ nanoparticles shown in Figure 2 have an average size of 1.8 ± 0.6 nm.

A control reaction, to test if the hydrogenation is influenced by mass-transfer limitations[63] even though the reaction is well stirred, was done in which the same $[Ir(1,5\text{-COD})Cl]_2$ and Bu_3N precursors were used, but each was concentration-doubled. The results, given in Figure S1 of the Supporting Information, show that the cyclohexene hydrogenation rate is doubled in comparison to that given in Figure 1b, demonstrating that the reaction is not under H_2 gas-to-solution mass-transfer limitations.[63]

The $Bu_3NH^+Cl^-$-stabilized $Ir(0)_n$ nanoparticles are active cyclohexene hydrogenation catalysts, providing an initial TOF of 1.1 s^{-1} at 22.0 ± 0.1 °C (Figure 1b). The nanoparticles can also be redispersed in acetone solution, retaining a TOF value of 0.2 s^{-1} at 22.0 ± 0.1 °C (Figure S2 in the SI) and yielding 25 000 total turnovers (TTOs) for cyclohexene reduction before deactivating via agglomeration (Figure S3 in the SI and in comparison to Figure S2). In short, compositionally relatively simple and relatively well-defined, catalytically active $Bu_3NH^+Cl^-$-stabilized $Ir(0)_n{\cdot}(Cl^-Bu_3NH^+)_a$ nanoparticles have been prepared from the in situ generated $Ir(0)_n{\cdot}H^+Cl^-$ in the presence of Bu_3N, as shown back in Scheme 2.

Demonstration of H^+Cl^- Removal from $Ir(0)_n{\cdot}(Cl^-Bu_3NH^+)_a$. To demonstrate the extent to which the weak, initially present labile ligand H^+Cl^- could be removed from the $Ir(0)_n{\cdot}(Cl^-Bu_3NH^+)_a$ nanoparticles, the solid particles were heated from 100 to 300 °C under He in a thermogravimetric analysis (TGA) experiment. The thermogravimetric analysis (TGA) data in Figure 3 show a weight loss of 8.6% between 25 and 120 °C, indicating that ≥98% of the HCl can be removed under the relatively mild TGA, ≤120 °C conditions. (It is likely that the other, ≤2% of HCl, was removed when the solvent and cyclohexane (resulting from the hydrogenation of cyclohexene) were removed under vacuum from the sample at room temperature, prior to the TGA analysis.) The 16.6% weight loss between 120 and 200 °C is attributed to partial removal of the resultant Bu_3N ligand (theoretical for the full loss of Bu_3N = 44.8%). Interestingly, the resultant Bu_3N-stabilized nanoparticles are partially, albeit not completely, stabilized against agglomeration when resuspended in acetone solution (see Figure S2 in the SI for details).

Of note here is that these results are interesting when considered in light of classic heterogeneous catalysis literature, where removal of Cl^- from the active metal surface is important because Cl^- is well known to affect catalytic rates, for example benzene hydrogenation over Ir/TiO_2 catalysts.[64] Additionally, Cl^- removal is crucial when trying to deconvolute trace Cl^- effects from the effects of changing facet ratios that accompany decreasing nanoparticle size.[65] In general, and despite extensive efforts to remove Cl^- quantitatively from supported catalysts, complete Cl^- removal from $MCl_x{\cdot}(H_2O)_n$ plus H_2 (and which in principle generates $M(0){\cdot}HCl$, not unlike the present syntheses) is a difficult task,[64,66,67] with, for example, demonstration of observable catalytic activity suppression at a Cl^-/Au molar ratio as low as 0.0006.[67] A compounding problem is that the waters of solvation can change the putative "$MCl_x{\cdot}(H_2O)_n$" to a more complex speciation that involves $MCl_{x-2y}O_y(H_2O)_{n-y}{\cdot}2y(HCl)$, not all of which are as readily or cleanly reducible to M(0) as is, for example, the $[(1,5\text{-COD})IrCl]_2$ precatalyst employed herein. However, by starting herein with the well-defined, already

DOI: 10.1021/acsomega.8b01569
ACS Omega 2018, 3, 14538−14550

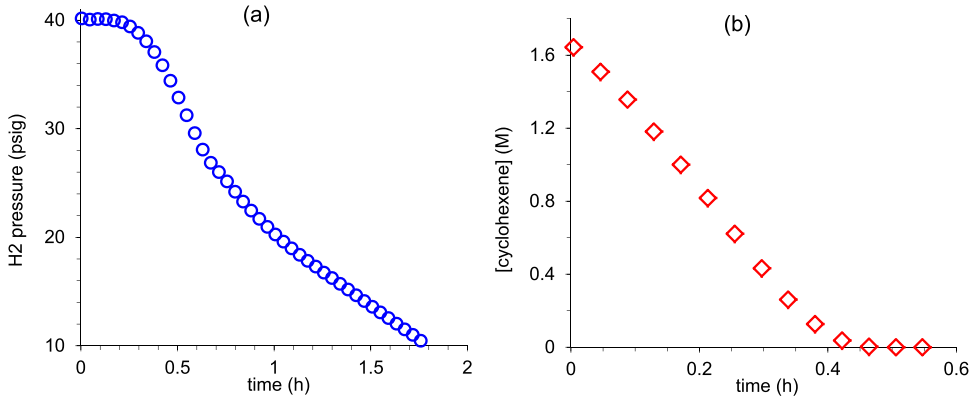

Figure 1. (a) Hydrogen uptake vs time plot for the hydrogenation of cyclohexene plus acetone and concomitant formation of iridium(0) nanoparticles starting with $[(1,5\text{-COD})IrCl]_2$ (1.2 mM Ir) and cyclohexene (1.65 M) in acetone at 22.0 ± 0.1 °C. Both cyclohexene and acetone undergo hydrogenation; the former is faster than the latter.[59] (b) Loss of cyclohexene versus time curve in the hydrogenation of 1.65 M cyclohexene and concomitant formation of Ir(0) nanoparticles starting with $[(1,5\text{-COD})IrCl]_2$ (1.2 mM Ir) and 1.2 mM Bu_3N in acetone at 22.0 ± 0.1 °C. A linear hydrogenation of cyclohexene starts with an initial turnover frequency (TOF) of 1.1 s^{-1}. The pressure rise in the initial part of both curves (not shown), due to the solvent vapor pressure reequilibration after 15 flushes of the reaction flask with H_2, has been corrected (and thereby removed from this curve as) by the precedented procedure described elsewhere.[61]

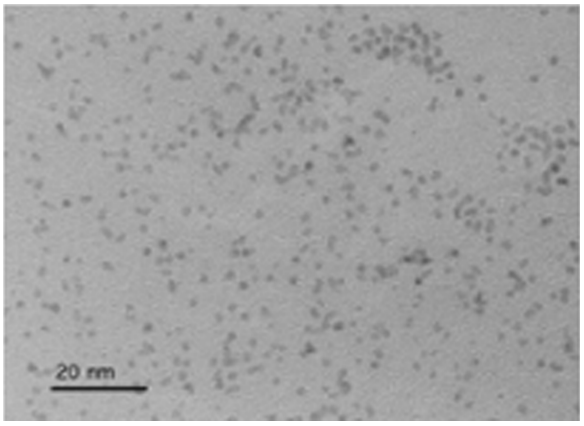

Figure 2. TEM image of $Ir(0)_n$ nanoparticles sample harvested after complete cyclohexene hydrogenation starting with $[(1,5\text{-COD})IrCl]_2$ (1.2 mM Ir) and 1.2 mM Bu_3N in acetone at 22.0 ± 0.1 °C. The average particle size is 1.8 ± 0.6 nm.

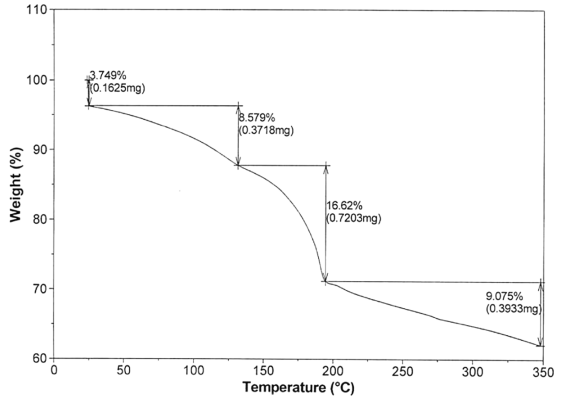

Figure 3. TGA of the $Bu_3NH^+Cl^-$-stabilized $Ir(0)_n$ nanoparticles formed during the reduction of 3.6 mM $[Ir(1,5\text{-COD})Cl]_2$ in the presence of 7.2 mM Bu_3N in acetone at 22 °C and under an initial pressure of 4.7 atm H_2 along with concomitant hydrogenation of an initial 1.65 M cyclohexene. The observed 8.6 wt % loss from 25 to 120 °C is attributable to the removal of ≥98% of the HCl present (i.e., 8.6% weight loss vs a theoretical 8.8% loss).

partially reduced (to Ir(I)) precursor $[(1,5\text{-COD})IrCl]_2$ (which, for example, lacks undesired waters of solvation), the reduction under H_2 proceeds cleanly and quantitatively to $Ir(0)\cdot H^+Cl^-$ according to the stoichiometry shown back in Scheme 1. The resultant, volatile HCl is then readily removable under relatively mild, ≤120 °C conditions (Scheme 4).

Scheme 4. Stoichiometry and Theoretical Weight Loss Percentages for the Removal of Volatile H^+Cl^- from $Ir(0)_n\cdot Cl^-Bu_3NH^+$ by Mild, ≤120 °C Heating

$$2/n\ Ir(0)_n + 2\ Bu_3NH^+Cl^- \xrightarrow{\text{Heat}} 2/n\ Ir(0)_n + 2\ Bu_3N + 2\ HCl$$

Theoretical wt% 46.4 % 44.8 % 8.8 %

Extension to Longer-Chain Amine-Stabilized Nanoparticles: $Dodec_3NH^+Cl^-$-Stabilized Nanoparticles $Ir(0)_n\cdot(Cl^-Dodec_3NH^+)_a$ from H_2 Reduction of $[Ir(1,5\text{-COD})Cl]_2$ in the Presence of $Dodec_3N$. To demonstrate the ready extension of the WLLL nanoparticle route to longer-chain amines that can, therefore, serve as enhanced stabilizers or render different nanoparticle solubility,[6] $[Ir(1,5\text{-COD})Cl]_2$ was reduced under H_2 in acetone solution at 22.0 ± 0.1 °C in the presence of tris(dodecyl)amine as an additional nanoparticle stabilizer as well as in the presence of 1.65 M cyclohexene (that, again, is completely hydrogenated as demonstrated by GC and NMR and, therefore, not available as an olefinic ligand stabilizer; Figure 4).

$Dodec_3NH^+Cl^-$-stabilized $Ir(0)_n$ nanoparticles show cyclohexene hydrogenation activity (initial TOF of ~1.4 s^{-1}) essentially the same as that of $Bu_3NH^+Cl^-$-stabilized $Ir(0)_n$ nanoparticles (initial TOF of 1.1 s^{-1}) at 22.0 ± 0.1 °C (Figure 4). The nanoparticles can be redispersed in acetone solution, retaining a TOF value of 0.2 s^{-1} in the second run of cylohexene hydrogenation at 22.0 ± 0.1 °C (Figure S4 in the SI). The TEM image (Figure 5) shows that the $Dodec_3NH^+Cl^-$-stabilized $Ir(0)_n$ nanoparticles have an average particle size of 1.8 ± 0.6 nm, the same within experimental error as the $Bu_3NH^+Cl^-$-stabilized $Ir(0)_n$ nanoparticles. These results demonstrate that changing the alkyl chain length by eight carbons from butyl to dodecyl has no significant

DOI: 10.1021/acsomega.8b01569
ACS Omega 2018, 3, 14538−14550

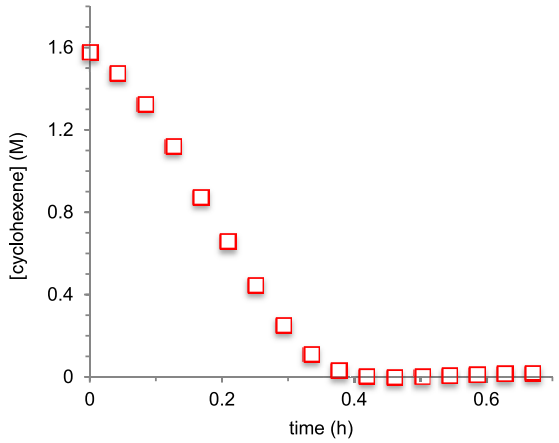

Figure 4. Loss of cyclohexene vs time curve in the H_2 reduction of $[(1,5\text{-COD})IrCl]_2$ (1.2 mM Ir) in the presence of 1.2 mM $Dodec_3N$ in acetone at 22.0 ± 0.1 °C along with concomitant complete hydrogenation of 1.65 M cyclohexene. The pressure rise observed in the initial part of the curve, due to the solvent vapor pressure reequilibration after 15 flushes of the reaction flask with H_2, has been corrected (and hence removed from this curve) by the precedented procedure described elsewhere.[61]

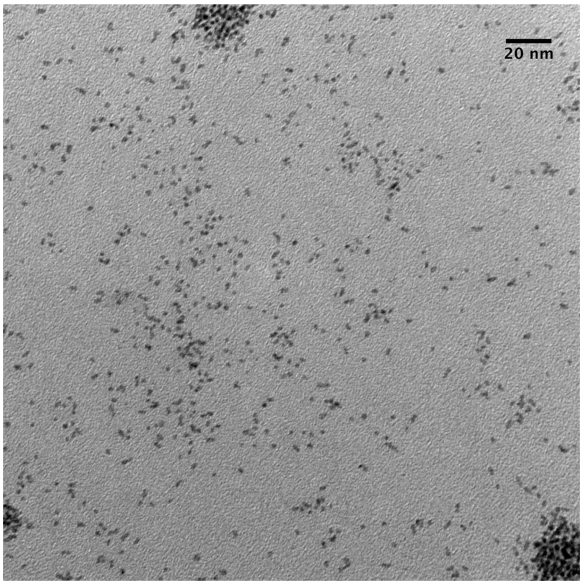

Figure 5. TEM image of $Ir(0)_n$ nanoparticles harvested after complete cyclohexene hydrogenation starting with $[(1,5\text{-COD})IrCl]_2$ (1.2 mM Ir) and 1.2 mM tris(dodecyl)amine, $Dodec_3N$ in acetone at 22.0 ± 0.1 °C. The average particle size is 1.8 ± 0.6 nm.

influence on the particle size or catalytic activity of the resultant $R_3NH^+Cl^-$-stabilized $Ir(0)_n$ nanoparticles.

$POct_3$-Stabilized $Ir(0)_n$ Nanoparticles, $Ir(0)_n\cdot(POct_3)_a(Cl^-H^+)_b$, from $[Ir(1,5\text{-COD})Cl]_2$ Plus $POct_3$. Starting with $[Ir(1,5\text{-COD})Cl]_2$ plus just 0.2 equiv $POct_3$ per mole of iridium in acetone, $Ir(0)_n\cdot(POct_3)_a(Cl^-H^+)_b$ nanoparticles were formed during the cyclohexene/acetone hydrogenation under H_2 at 22.0 ± 0.1 °C (Figure 6a). Trioctylphosphine was picked based on a suggestion from our collaborator Prof. A. Karim and because it is a strongly binding ligand with a perhaps surprisingly small Tolman cone angle of 107° (in comparison to PR_3 (R = Et, Pr, Bu) cone angles that are all 132°).[68] Importantly, adding just 0.2 equiv $POct_3$ per mole of Ir to the starting $[Ir(1,5\text{-COD})Cl]_2$ precatalyst solution yields stable iridium(0) nanoparticles that are still active hydrogenation catalysts. In short, the $Ir(0)_n\cdot(Cl^-H^+)_b$ WLLL concept leads to the ready preparation of $Ir(0)_n\cdot(POct_3)_a(Cl^-H^+)_b$ nanoparticles with an approximately (low level) minimum amount of added ligand, L = ($POct_3$) in this case, which yields a narrow, 1.5 ± 0.2 nm dispersion of catalytically active $Ir(0)_n$ nanoparticles with no visibly or TEM-discernable bulk metal.

Figure 6b shows TEM image of the sample harvested after the complete hydrogenation of cyclohexene and acetone (22 h) exhibiting the formation of highly dispersed Ir(0) nanoparticles. The GC determination of 1.0 ± 0.1 equiv of cyclooctane evolution per mole of Ir after 22 h indicates the complete reduction of the (1,5-COD)Ir(I)-containing precursor to Ir(0) when the nanoparticle sample harvested. The average particle size is 1.5 ± 0.2 nm according to the histogram in Figure 6c. The comparison of the particle size of $Ir(0)_n\cdot(POct_3)_a(Cl^-H^+)_b$ to that of $Bu_3NH^+Cl^-$- or $Dodec_3NH^+Cl^-$-stabilized nanoparticles (1.8 ± 0.6 nm) is consistent with the effect of the stronger binding $POct_3$ phosphine ligand yielding an on average smaller, ≥3 fold-narrower size distribution of $Ir(0)_n\cdot(POct_3)_a(Cl^-H^+)_b$ nanoparticles.

Noteworthy here is that ligand-based control of nanoparticle sizes and size distributions is an important current research topic.[9,45,69−71] The $Ir(0)_n\cdot(POct_3)_a(Cl^-H^+)_b$ system developed herein is important in this regard because well-formed and size-controlled $Ir(0)_{\sim 150}$ nanoparticles[a,72,73] are formed from even low, 0.2 equiv ligand-to-Ir ratios—implying, in turn, that ligand-to-Ir ratios between 0.2 and ≥1.0 should be studiable by in-progress small-angle X-ray scattering (SAXS) and other efforts.

Isolable, HCl-free, Minimally Ligated $Ir(0)_n\cdot(POct_3)_{0.2n}$ Nanoparticles. Significantly, trioctylphosphine-stabilized $Ir(0)_n\cdot(POct_3)_{0.2n}$ nanoparticles, with only 0.2 equiv of $P(Oct)_3$ and testing ≥99% free of HCl, could be isolated as a powder by removing HCl and the acetone solvent under vacuum. It is noteworthy that these isolated Ir(0) nanoparticles are redispersible in acetone and other organic solvents with good catalytic activity: Figure 7a shows the H_2 uptake versus time plot cyclohexene plus acetone hydrogenation using the isolated $Ir(0)_n$ nanoparticles formed from a first run of cyclohexene/acetone hydrogenation. Compared to the $Ir(0)_n\cdot(POct_3)_a(Cl^-H^+)_b$ nanoparticles (Figure 6c, where the mean particle size is 1.5 ± 0.2 nm, i.e., ±15%), the $Ir(0)_n\cdot(POct_3)_a$ nanoparticles do exhibit a somewhat broadened size distribution (Figure 7c, the mean particle size = 1.4 ± 0.4 nm, i.e., ±28%), not unexpectedly because of some agglomeration during the isolation and redispersion processes.

However and significantly, HCl has been largely removed as demonstrated by the very slow hydrogenation of acetone seen in Figure 7 (~0.91 psig H_2 loss/h), HCl being a known requirement for facile acetone hydrogenation (i.e., by the same precatalyst and under essentially identical conditions[59]).

Independently, confirming evidence for the removal of HCl at the >99% level (i.e., from HCl-containing, $Ir(0)_n\cdot(POct_3)_{0.2n}(Cl^-H^+)_b$ nanoparticles) to give the novel, essentially HCl-free $Ir(0)_n\cdot(POct_3)_{0.2n}$ nanoparticles is provided by treatment of the isolated product with a 1.2 mM $AgBF_4$ solution in acetone (the same concentration as the initial $[(1,5\text{-COD})IrCl]_2$ precursor concentration). No visually observable precipitation of AgCl is seen, confirming the expected removal of HCl during the evacuation step to yield the HCl-free $Ir(0)_n\cdot(POct_3)_{0.2n}$ product. To establish the limit

DOI: 10.1021/acsomega.8b01569
ACS Omega 2018, 3, 14538−14550

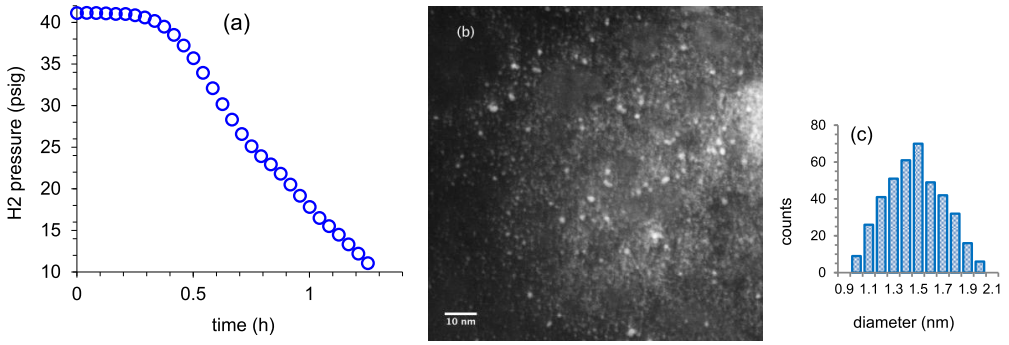

Figure 6. (a) Hydrogen uptake vs time plot for the hydrogenation of cyclohexene/acetone and concomitant formation of $Ir(0)_n$ nanoparticles starting with $[(1,5\text{-COD})IrCl]_2$ (1.2 mM Ir) plus 0.2 equiv $POct_3$ and cyclohexene (1.65 M) in acetone at 22.0 ± 0.1 °C. The pressure rise observed in the initial part of curve, due to the solvent vapor pressure reequilibration after 15 flushes of the reaction flask with H_2, has been corrected (and hence removed from this curve) by the precedented procedure described elsewhere.[61] (b) Bright-field scanning transmission electron microscopy (STEM) image and (c) the corresponding particle size histogram of $Ir(0)_n{\cdot}(POct_3)_a(Cl^-H^+)_b$ nanoparticles in the sample harvested after 22 h hydrogenation (1.0 ± 0.1 equiv cyclooctane had evolved as determined by GC). The mean diameter of Ir(0) nanoparticles is 1.5 ± 0.2 nm (i.e., ±15%).

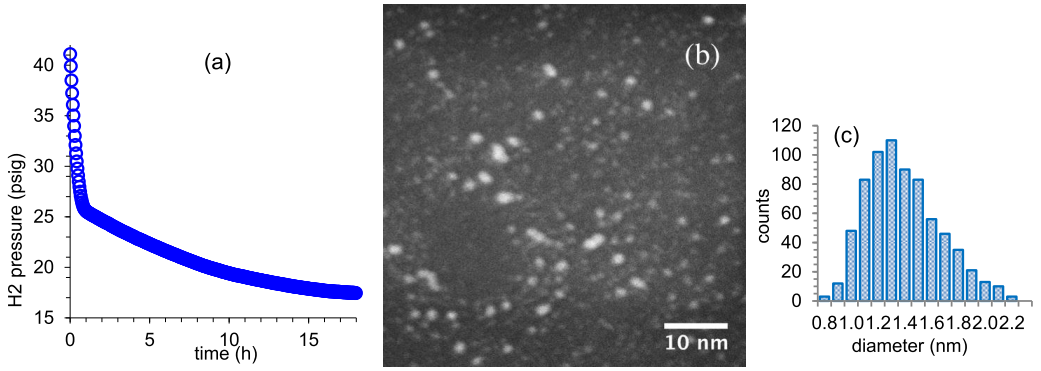

Figure 7. (a) Hydrogen consumption vs time plot for the hydrogenation of cyclohexene (the fast part of the H_2 pressure loss curve) then acetone (the slower, subsequent part of the hydrogenation curve) using the redispersed $Ir(0)_n{\cdot}(POct)_{0.2n}$ nanoparticles formed from a first run of cyclohexene/acetone hydrogenation (i.e., formed starting with $[(1,5\text{-COD})IrCl]_2$ (1.2 mM Ir) plus 0.2 equiv $POct_3$ and cyclohexene (1.65 M) in acetone at 22.0 ± 0.1 °C). The Ir(0) nanoparticles were isolated by removing the volatiles including HCl in vacuum and then redispersed in acetone for this second hydrogenation. The pressure rise observed in the initial part of the curve, due to the solvent vapor pressure reequilibration after 15 flushes of the reaction flask with H_2, has been corrected (and hence removed from this curve) by the precedented procedure described elsewhere.[61] (b) Bright-field STEM image of the sample harvested after 22 h hydrogenation and (c) the corresponding particle size histogram of $Ir(0)_n{\cdot}(POct_3)_{0.2n}$ nanoparticles. Mean diameter of Ir(0) nanoparticles is 1.4 ± 0.4 nm (i.e., ±28%).

of Cl^- (and thus HCl) detectability in the added Ag^+ experiment, a control was performed with 0.012 mM $Bu_4N^+Cl^-$ (i.e., 1% relative to 1.2 mM Ir) plus 1.2 mM $AgBF_4$ in acetone: a readily visualized AgCl precipitate is seen, in turn showing that even a 1% level of residual Cl^- would have been easily detected by the above simple, effective, AgCl precipitation test. Taken together, the results demonstrate that the HCl has been removed at the >99% level from the $Ir(0)_n{\cdot}(POct_3)_{0.2n}(Cl^-H^+)_b$ nanoparticle sample. The resultant desired, isolable, and redispersible, yet still highly catalytically active $Ir(0)_n{\cdot}(POct_3)_{0.2n}$ nanoparticles possess a by-design low level of ligation that, however, is sufficient to allow the nanoparticles to be both isolated and then redispersed.

Note that a roughly average $Ir(0)_{\sim 150}$ nanoparticle has ca. 0.6 of its total Ir atoms on the surface of the nanoparticle so that one expects the 0.2 equiv of $POct_3$ present to be tightly bound in the as-formulated, $Ir(0)_n{\cdot}(POct_3)_{0.2n}$ nanoparticles. While clearly much more remains to be done further characterizing and studying the $Ir(0)_n{\cdot}(POct_3)_{0.2n}$ nanoparticles, including their quantitative poisoning behavior,[74,75] there can be little doubt that minimally ligated, WLLL-derived nanoparticles such as $Ir(0)_n{\cdot}(POct_3)_{0.2n}$ hold considerable promise in catalysis and other applications. A wide range of other ligands, mixed ligand combinations, and other surface-directed chemistry should now be possible by the same route using the $Ir(0)_n{\cdot}(Cl^-H^+)_b$ WLLL approach, as well as through further reactions of the isolable $Ir(0)_n{\cdot}(POct_3)_{0.2n}$ nanoparticles as Scheme 2 begins to make apparent. Ligands of interest include those identified in prior, valuable studies by others.[9,45,69−71]

γ-Al_2O_3-Supported, Labile Ligand Nanoparticles-Derived $Ir(0)_n/(\gamma\text{-}Al_2O_3)(Cl^-H^+)$. The $Ir(0)_n{\cdot}H^+Cl^-$ nanoparticle is also applicable to the synthesis of supported heterogeneous catalysts[76−81] (i.e., and as was hypothesized to be what was occurring when molecular sieves were added to $Ir(0)_n{\cdot}H^+Cl^-$ nanoparticles previously[59]). The work that follows closely mirrors our previously published work,[82−85] but ties it into the $Ir(0)_n{\cdot}H^+Cl^-$ nanoparticle WLLL and synthon concepts and, hence, is included in this report for the sake of completeness.

As before,[82,83,85] a supported version of the precatalyst, $[Ir(1,5\text{-COD})Cl]/\gamma\text{-}Al_2O_3$, was isolated first and then reduced under H_2, in acetone, and in the presence of cyclohexene (Scheme 5 (top)). A cyclohexene reporter reaction, shown in the bottom half of Scheme 5, allows one to monitor the

DOI: 10.1021/acsomega.8b01569
ACS Omega 2018, 3, 14538−14550

Scheme 5. Stoichiometry, Synthesis Conditions, and Cyclohexene Hydrogenation Reaction of Interest for $Ir(0)_n/(\gamma\text{-}Al_2O_3)(Cl^-H^+)$-Supported Nanoparticle Heterogeneous Catalyst Formation[82]

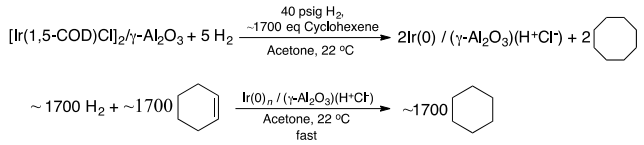

nanoparticle formation reaction.[82,83,85] The stoichiometry of the reaction was confirmed as before[82] by demonstrating (gas–liquid chromatography (GLC), and NMR) the evolution of 1.0 ± 0.1 equiv of cyclooctane.[82]

The observed sigmoidal kinetics along with the fit to the Finke–Watzky two-step mechanism of slow continuous nucleation (A → B, rate constant k_1), followed by fast autocatalytic surface growth (A + B → 2B, rate constant k_2) of this nanoparticle formation reaction,[60] implies that near-monodisperse (≤±15% size dispersion[14]) nanoparticles should be formed.[83,86] Indeed, the resultant supported nanoparticles are 2.9 ± 0.4 nm (±14%) and are an active (24 ± 5 turnovers/s at 22.0 ± 0.1 °C) and long-lived catalyst (360 000 total catalytic turnovers of cyclohexene hydrogenation).[83] These results both verify our prior work[83,84] and demonstrate that the $Ir(0)_n{\cdot}H^+Cl^-$ WLLL nanoparticle approach is of value in preparing supported-nanoparticle heterogeneous catalysts, specifically $Ir(0)_n/(\gamma\text{-}Al_2O_3)(Cl^-H^+)$.

These catalysts contain only H^+Cl^-, cyclohexane, acetone solvent, and the support as possible ligands. The controlled reaction stoichiometry[82] and resultant product are therefore important aspects of the synthetic route to the present WLLL nanoparticles. The WLLL nanoparticle synthetic route and resultant supported nanoparticle have several advantages (i.e., compared to first forming the nanoparticles, depositing them on a support, and then trying—largely unsuccessfully[16−25]—to remove all of the stabilizing ligands[86−88]): (i) the WLLL approach does not require the use of polymer or other, excessive or strong-binding ligands that can poison catalysis and block surface sites needed for other applications; (ii) the WLLL approach eliminates separate nanoparticle isolation and deposition steps, and additionally (iii) the fit of the sigmoidal kinetics to the two-step mechanism imply that nine insights into the synthesis of nanoparticle catalysts[86] should also apply to the resultant products, including the following four chosen for illustration here: (a) the formation of near-monodisperse particles;[82] (b) the ability of the added ligands to attach to growing nanoparticle facets and induce shape control,[82] (c) size control over the resultant supported-nanoparticle heterogeneous catalyst;[89] and (iv) rational syntheses of all possible geometric isomers of, for example, bi- or multimetallic nanoparticles.[82] Overall, the results offer strong support for the efficacy of the WLLL nanoparticle route to supported-nanoparticle heterogeneous catalysts.[83,85]

Additional Possible Applications of WLLL Nanoparticles. A look back at Scheme 2 shows a couple of additional—among many other conceivable—uses of WLLL nanoparticles. One is to make the nanoparticles in ionic liquids, well-known excellent stabilizers of nanoparticles, an application that already has good precedent,[34,90−94] particularly in Dupont and co-worker's seminal studies starting with $[Ir(1,5\text{-}COD)Cl]_2$ to form biphasic, ionic liquid-stabilized $Ir(0)_n$ nanoparticle alkene hydrogenation catalysts.[91]

Using volatile buffers as meta-stabilizing ligands is another, interesting, conceivable way to make a different version of WLLL nanoparticles (Scheme 2) vide supra. The idea here is to use known volatile buffers, such as ammonium carbonate ($(NH_4)_2CO_3$) and ammonium hydrogen carbonate ($(NH_4)HCO_3$), as potential meta-stabilizers. If they could provide sufficient meta-stabilization, then these salts have the desirable, well-established property of being volatile (buffers) so that they could, then and in principle, conceivably be readily and completely removed under mild heat and vacuum conditions as shown in eq 1 (neat ammonium carbonate decomposing according to eq 1 at 60 °C and 1 atm, and in dodecane solution at 100 °C, for example[95,96])

$$(NH_4)_2CO_3 \xrightarrow{\text{heat}} 2NH_3 + CO_2 + H_2O \quad (1)$$

$$(NH_4)HCO_3 \xrightarrow{\text{heat}} NH_3 + CO_2 + H_2O \quad (2)$$

This idea intrigued us enough that we tested it experimentally, if just initially. The first problem we ran into is that neither ammonium carbonate nor ammonium hydrogen carbonate is soluble in acetone or propylene carbonate, the two organic solvents we have emphasized for our nanoparticle preparations. However, using $(Bu_3NH)_2CO_3$ in acetone generated in situ from $[(1,5\text{-}COD)Ir(MeCN)_2]_2CO_3$ with 1 equiv Bu_3N (added as the base needed to scavenge H^+ generated in the H_2 reduction of the $[(1,5\text{-}COD)Ir(I)^+]$ moiety) followed by reduction under H_2 did yield a brown, nanoparticle-containing solution, which exhibited 2.2 ± 0.7 nm particles by TEM. Unfortunately, once taken to vacuum to isolate them, the "$Ir(0)_n{\cdot}(CO_3)(Bu_3NH)_2$" nanoparticles are not redispersable in acetone (see the SI for details), and hence apparently not sufficiently stabilized to be isolable. Accordingly, the "volatile buffer" approach is labeled in Scheme 2 as "undemonstrated", but included here because of the interesting nature of the volatile buffer concept and the hope that suitable variations of it might work based on the creative ideas and efforts of others.

CONCLUSIONS

In conclusion, the example of $Ir(0)_n{\cdot}H^+Cl^-$ as a WLLL, isolable, yet effectively coordinatively unsaturated nanoparticle system has been illustrated and expanded herein based on H_2 reduction of a $[Ir(1,5\text{-}COD)Cl]_2$ precatalyst in acetone. The use of the meta-stable $Ir(0)_n{\cdot}H^+Cl^-$ as a valuable synthetic structural unit/building block was illustrated by the preparation of five specific nanoparticle products: $Ir(0)_n{\cdot}(Cl^-Bu_3NH^+)_a$, $Ir(0)_n{\cdot}(Cl^-Dodec_3NH^+)_a$, $Ir(0)_n{\cdot}(POct_3)_a(Cl^-H^+)_b$, $Ir(0)_n{\cdot}(POct_3)_a$, and the $\gamma\text{-}Al_2O_3$-supported heterogeneous catalyst, $Ir(0)_n{\cdot}(\gamma\text{-}Al_2O_3)_a(Cl^-H^+)_b$. In the case of the $Ir(0)_n{\cdot}(Cl^-Bu_3NH^+)_a$ nanoparticles, it was shown that HCl could be quantitatively (≥98%) removed by mild heating, opening the door for removal of the volatile HCl in cases where doing so is desired. Removing HCl from $Ir(0)_n{\cdot}(POct_3)_{0.2}(Cl^-H^+)_b$ in vacuum at 30 °C yields isolable and redispersible $Ir(0)_n{\cdot}(POct_3)_{0.2}$ nanoparticles ≥99% free of HCl, nanoparticles that can be weighed out as a solid for any desired application, and nanoparticles that retain their high catalytic activity post redispersion in acetone.

The case of the $POct_3$-stabilized nanoparticles, $Ir(0)_n{\cdot}(POct_3)_{0.2}$, is especially significant in that just 0.2 equiv of $POct_3$ was demonstrated to provide well-formed, reasonably

DOI: 10.1021/acsomega.8b01569
ACS Omega 2018, 3, 14538−14550

well-stabilized, size-controlled $Ir(0)_{\sim 150}$ nanoparticles—thereby opening up in-progress quantitative kinetic, mechanistic, SAXS, and other studies of size control as a function of precisely known amounts of added ligand, L, which start from ≪1 equiv of L per metal present in $Ir(0)_n \cdot (POct_3)_{0.2}$.

Presented in Scheme 2 are additional possibilities for exploiting the WLLL nanoparticle concept, for example, the use of other, readily removable ligands such as volatile buffers. The ready commercial availability of labile ligand organometallic precursors/precatalysts analogous to $[(1,5\text{-COD})\mathbf{Ir}Cl]_2$ such as $[(1,5\text{-COD})\mathbf{Rh}Cl]_2$, $(1,5\text{-COD})\mathbf{Pt}Cl_2$, $\mathbf{Ru}(COD)(COT)$, as well as other precursors that one can imagine to labile ligand nanoparticles fuels our hope that others will add to and expand the examples and applications of WLLL nanoparticles in their own research.

EXPERIMENTAL SECTION

Materials. All commercially obtained reagents were used as received unless otherwise noted. All solvents were stored in a ≤1 ppm O_2 drybox prior to use. Acetone packed under nitrogen was purchased from Burdick & Jackson (water content <0.5%). Cyclohexene (Aldrich, 99%) was freshly distilled over sodium metal under argon and stored in a predried glass bottle. $[Ir(1,5\text{-COD})Cl]_2$ (STREM), tris(dodecyl)amine (Aldrich, 97%), trioctylphosphine (Aldrich, 97%), and tributylamine (Aldrich, ≥99.5%) were stored in a drybox. Solutions (1.0 M) of proton sponge (Aldrich) in acetone were freshly made. Acidic γ-Al_2O_3 (Aldrich) with a surface area of 155 m^2/g was dried at 160 °C for 24 h and stored in the drybox prior to use. CD_2Cl_2 (Cambridge Isotope Laboratories) from 1 mL glass ampoules were transferred into the drybox for NMR sample preparation. H_2 gas was purchased from General Air in >99.5% purity and passed through O_2 and H_2O scavenging traps (Trigon Technologies) before use to pressurize Fisher-Porter (FP) bottle reactors (vide infra).

Analytical Instrumentation and Procedures. Unless otherwise reported, all reaction solutions were prepared under oxygen and moisture-free conditions in a Vacuum Atmospheres nitrogen-filled drybox. The O_2 level (≤1 ppm O_2) was continuously monitored by a Vacuum Atmospheres O_2 sensor. Gas−liquid chromatography (GLC) was performed using a Hewlett-Packard 5890 Series II GC with an flame ionization detector equipped with a 30 m (0.25 mm i.d., 25 μm film) Supelco SPB-1 column coupled with a Hewlett-Packard 3395 integrator. The GLC parameters are: initial temperature, 50 °C; initial time, 3 min; ramp, 10 °C/min; final temperature, 160 °C, final time, 16 min; injector port temperature, 180 °C; detector temperature, 200 °C; and injection volume, 2 or 4 μL. High-resolution ^1H (300.115 MHz) and ^{13}C (75.472 MHz) NMR spectra were taken on a Varian INOVA-300 spectrometer. Thermogravimetric analysis (TGA) was carried out in a TA Instruments TA 2950 thermogravimetric analyzer (with integrated Balzers mass spectrometer) using Pt pans, in a He purged atmosphere. The ramping rate used was 2 °C/min until the appropriate temperature was reached. TEM analysis was done using a Philips CM-12 TEM with a 70 μm lens operating at 100 kN and with a 2.0 Å point-to-point resolution, and a JEOL JEM-2100F transmission electron microscope operating at 200 kV was used to take bright-field STEM images of iridium(0) nanoparticles deposited on an silicon nitride grid (Ted Pella, Inc.). TEM images were analyzed by using Public-Domain Image-Processing Program.[97] Typically, TEM pictures of each sample were taken at three different magnifications (100, 200, and 430 K) to obtain information about the sample.

Hydrogenation Apparatus and Data Handling. Hydrogenation experiments were carried out in a custom-built, previously described[73] apparatus to continuously monitor hydrogen pressure loss. Briefly, the apparatus consists of a Fisher-Porter (FP) bottle modified with Swagelok TFE-sealed quick-connects to both a H_2 line and an Omega PX621 pressure transducer. The pressure transducer is interfaced to a PC via an Omega D1131 5 V A/D converter with an RS-232 connection. Pressure uptake data were collected using LabView 7.1 and analyzed using Origin 7.0 when the data could be fit to the known two-step autocatalytic mechanism.[60] The hydrogen uptake curves were converted to cyclohexene consumption curves before analyzing via Orgin 7.0, which is done by using the known 1:1 H_2 to cyclohexene stoichiometry and the previously established cyclohexene reporter reaction kinetic method.[60]

Preparation of $Ir(0)_n \cdot H^+Cl^-$ Nanoparticles for Acetone Hydrogenation. As previously described and reproduced as a control experiment,[59] in a 2 dram glass vial, 1.2 mg (3.6 μmol of Ir) of the precatalyst $[Ir(1,5\text{-COD})Cl]_2$ was weighed and dissolved in 0.5 mL (6.7 mmol) of acetone (added with a 1.0 mL gastight syringe), to yield a clear, yellow solution. The solution was then transferred via a disposable polyethylene pipet into a new 22 × 175 mm^2 Pyrex culture tube containing a new 5/16 in. × 5/8 in. Teflon-coated stir bar. The culture tube was then sealed inside the FP bottle, brought outside the drybox, placed in a constant-temperature water-circulating bath at 22.0 ± 0.1 °C, and attached via Swagelok TFE-sealed quick-connects to the hydrogenation line described in the above section. Stirring was started (>600 rpm; this stirring rate is important to avoid H_2 gas-to-solution mass-transfer limitations), and the FP bottle was then purged 15 times with hydrogen (15 s per purge), stirred vigorously for an additional 30 s, and then $t = 0$ was noted.

Preparation of $Ir(0)_n \cdot Bu_3NH^+Cl^-$-Stabilized Nanoparticles. In the drybox, 1.8 μmol (3.6 μmol in Ir) $[Ir(1,5\text{-COD})Cl]_2$ was weighed into a 2 dram predried glass vial. Subsequently, 2.5 mL of acetone and 0.5 mL of cyclohexene were added via gastight syringes to the 2 dram vial. Next, 3.6 μmol tributylamine was added to the vial, and the resulting solution was mixed with a disposable polyethylene pipette and transferred into a new borosilicate culture tube (22 × 175 mm^2) with a new 5/8 in. × 5/16 in. Teflon-coated octagon-shaped stir bar. A standard conditions hydrogenation was performed following the previously developed procedure.[73]

Preparation of $Ir(0)_n \cdot POct_3$-Stabilized Nanoparticles. Preparation of trioctylphosphine stock solution: In the drybox, 1.0 mmol $POct_3$ was transferred via a 1 mL gastight syringe from the bottle (Aldrich, 97%) into a septum-sealed, 20 mL bottle by weighing the amount of transferred liquid. Then, 9.6 mL of cyclohexane was added to the bottle. The total volume of solution was 10.0 mL, and the concentration of $POct_3$ was 100 mM. A 100 μL aliquot of this solution was transferred into a 5.0 mL volumetric flask, and the volume was completed to 5.0 mL by adding cyclohexane. The $POct_3$ concentration of this solution was 2.0 μmol/mL. A preselected aliquot of this solution, to achieve the desired concentrations noted in experiments in the main text, was then added to the precatalyst solution.

In a 2 dram glass vial, 1.2 mg (3.6 μmol of Ir) of the precatalyst $[Ir(1,5\text{-COD})Cl]_2$ was weighed and dissolved in

DOI: 10.1021/acsomega.8b01569
ACS Omega 2018, 3, 14538−14550

2.14 mL of acetone to yield a clear, yellow solution. The solution was then transferred via a disposable polyethylene pipet into a new 22 × 175 mm^2 Pyrex culture tube containing a new 5/16 in. × 5/8 in. Teflon-coated stir bar. To this solution, a 360 μL aliquot of the trioctylphosphine solution (360 μL × 2.0 μmol/mL = 0.72 μmol $POct_3$) and 0.5 mL of cyclohexene were added. A standard conditions hydrogenation was performed following the previously developed procedure.[73]

After the first run of hydrogenation, the FP bottle was taken into the drybox. The solution in the culture tube was connected to vacuum and brought to dryness for 3 h (10^{-1} Torr, 25 °C). The residue in the culture tube was redispersed in 2.5 mL of acetone. After addition of 0.5 mL of cyclohexene, the culture tube was then sealed inside the FP bottle, brought outside the drybox, placed in a constant-temperature water-circulating bath at 22.0 ± 0.1 °C, and attached via Swagelok TFE-sealed quick-connects to the hydrogenation line. A standard conditions hydrogenation was then performed following the previously developed procedure.[73]

Catalyst Lifetime Experiments from $[Ir(1,5\text{-}COD)Cl]_2$ with Added Bu_3N. The catalyst lifetime experiment was performed identically to those previously published.[59] In the drybox, 0.72 μmol $[Ir(COD)Cl]_2$ and 0.72 μmol Bu_3N were dissolved in 4.5 mL of acetone added via a 10 mL gastight syringe. The resulting solution was mixed using a disposable polyethylene pipette and transferred into a new borosilicate culture tube (22 × 175 mm^2) with a new 5/8 in. × 5/16 in. Teflon-coated octagon-shaped stir bar. Next, 4.5 mL (44 mmol, corresponding to a maximum of 61 000 turnovers) of cyclohexene was added to the culture tube and then the FP bottle was sealed and brought out of the drybox. The FP reactor was purged and set to 40 psig, as described above.

The reaction was monitored by periodically withdrawing aliquots of the reaction solution for ^1H NMR spectroscopy. This monitoring was accomplished by sealing the FP bottle, disconnecting it from the hydrogenation line and then transferring the vessel back into the drybox. Aliquots were removed inside the drybox by using a 9 in. glass Pasteur pipette inserted into the reaction solution and drawing out 0.05 mL of aliquots. The aliquot was then added to 1 g of $CDCl_2$ in an individual glass ampoule and mixed using a Pasteur pipette, which was then transferred to an NMR tube. The FP bottle was then resealed, taken out of the drybox, reconnected to the H_2 line, and the above-noted purge cycle with H_2 to restart the hydrogenation reaction was repeated. The NMR tube containing the reaction aliquot was sealed and brought out of the drybox, and a ^1H NMR spectrum was obtained.

Preparation of $Ir(0)_n/\gamma\text{-}Al_2O_3$-Stabilized Nanoparticles. The precatalyst solutions were prepared in the drybox using preselected $[Ir(1,5\text{-}COD)Cl]$/support weight-to-weight ratios following the procedure described elsewhere.[82] Each individual sample was then transferred via a disposable polyethylene pipette into the new borosilicate culture tube (22 × 175 mm^2) containing a new 5/8 in. × 5/16 in. Teflon-coated octagon-shaped stir bar. A standard conditions hydrogenation was performed following the previously developed procedure.[73]

Preparation of TEM Grids. Following the hydrogenation of cyclohexene (and acetone) and the formation of nanoparticles, the FP bottle was sealed, disconnected from the H_2 line, and transferred into the drybox. The reaction solution was quantitatively transferred with a disposable polyethylene pipette into a clean, 5 mL screw-capped glass vial. The solution was dried under vacuum of $<10^{-1}$ Torr at 30 °C for 3 h and then the glass vial was sealed and brought out of the drybox. The dry nanoparticle samples were sent as solids (in screw-capped glass vials) to Clemson University for TEM investigation. There, 1 mL of acetonitrile was added just before the TEM was obtained. A drop of this solution was then redispersed on a chloroform-cleaned, carbon-coated Cu TEM grid. $Ir(0)_n/\gamma\text{-}Al_2O_3$ TEM samples were prepared by dipping a TEM grid into the resultant nanoparticle solution for 5 s.

The solutions used for the preparation of grids for bright-field STEM images were exactly the same ones prepared in the respective sections above. At the end of complete hydrogenation of cyclohexene (and acetone), the FP bottle was detached from the hydrogenation line via its quick-connects, brought back into the drybox, and its acetone solution was quantitatively transferred with a disposable polyethylene pipette into a clean, 2 dram glass vial. A 0.2 mL aliquot of the solution was added into 1 mL 2-butanone in the 2 dram vial for dilution, 0.1 μL of the diluted solution was dropped via a micropipette on a silicon nitride grid, and the excess liquid was removed by quickly wicking away from the lower edge of grid. The grids were left in the drybox for drying for a minimum of 2 h prior to start with the electron microscopy analysis.

Thermogravimetric Analysis Sample Preparation for $[(1,5\text{-}COD)IrCl]_2$ with Bu_3N. Two scaled up hydrogenations containing 3.6 μmol $[(1,5\text{-}COD)IrCl]_2$ and 7.2 μmol Bu_3N, 2.5 mL of acetone, and 0.5 mL of cyclohexene were performed. The nanoparticle solutions were transferred into the drybox and combined. The volatiles (acetone and cyclohexane) were gently removed under vacuum of $<10^{-1}$ Torr at 30 °C in an effort to minimize the possible loss of Bu_3N and HCl in this necessary step. The black residue was then transferred into an aluminum TGA capsule and sealed in the drybox by mechanical press. Immediately prior to TGA analysis, a hole was placed in the capsule and the sample pan was placed in the TGA for analysis.

■ ASSOCIATED CONTENT

Supporting Information

The Supporting Information is available free of charge on the ACS Publications website at DOI: 10.1021/acsomega.8b01569.

Literature reports of naked nanoparticles; plot of cyclohexene loss versus time for the hydrogenation of 1.65 M cyclohexene starting with 3.6 μmol $[(1,5\text{-}COD)IrCl]_2$ and 7.2 μmol Bu_3N; plot of cyclohexene loss vs time for the second run of hydrogenation of 1.65 M cyclohexene by using isolated Ir(0) nanoparticles and TEM imaging of sample harvested after reaction; evolution of the total turnovers (TTOs) of cyclohexene hydrogenation and TEM image of the sample harvested after the catalytic lifetime measurement; plot of cyclohexene loss vs time in the second run of hydrogenation of 1.65 M cyclohexene using the Ir(0) nanoparticles formed initially, and in a first run of cyclohexene hydrogenation starting with 0.6 mM $[(1,5\text{-}COD)IrCl]_2$ and 1.2 mM $dodecyl_3N$; attempted formation of volatile buffer-stabilized Ir(0) nanoparticles using alkylammonium carbonate; attempted formation of tetrabutylammonium carbonate-stabilized Ir(0) nanoparticles; attempted formation of tributylammonium

DOI: 10.1021/acsomega.8b01569
ACS Omega 2018, 3, 14538−14550

carbonate-stabilized Ir(0) nanoparticles in acetone; plot of cyclohexene loss versus time curve for the hydrogenation of 1.65 M cyclohexene starting with 0.6 mM $[(1,5\text{-COD})Ir]_2CO_3$ and 0.6 mM $[Bu_3NH]_2CO_3$; attempted formation of tributylammonium carbonate-stabilized Ir(0) nanoparticles using $[(1,5\text{-COD})Ir(CH_3CN)_2]_2CO_3$ as precursor in acetone; plot of cyclohexene loss versus time in the hydrogenation of 1.65 M cyclohexene starting with 0.6 mM $[(1,5\text{-COD})Ir]_2CO_3$ and 1.2 mM proton sponge and TEM image of the sample harvested after reaction; and TGA of the tributylammonium carbonate-stabilized Ir(0) nanoparticles obtained from the hydrogenation of $[(1,5\text{-COD})Ir(CH_3CN)_2]_2CO_3$ and 1.2 mM Bu_3N (PDF)

AUTHOR INFORMATION

Corresponding Author

*E-mail: Richard.Finke@colostate.edu.

ORCID

Saim Özkar: 0000-0002-6302-1429

Richard G. Finke: 0000-0002-3668-7903

Notes

The authors declare no competing financial interest.

ACKNOWLEDGMENTS

This work was supported by Colorado State University's U.S. Department of Energy (DOE), Office of Science, Office of Basic Energy Sciences, Division of Chemical Sciences, Geosciences & Biosciences, via DOE Grant SE-FG402-03ER15453.

ADDITIONAL NOTE

[a]The average size of the iridium(0) nanoparticles was estimated on the basis of an assumed face-centered cubic structure for iridium: $n = (N_0\rho(4/3)\pi(D/2)^3)/W$,[73] where n is the number of Ir atoms, $N_0 = 6.022 \times 10^{23}$ mol^{-1}, ρ is the room-temperature density of iridium (22.5 g/cm^3), D is the diameter of iridium nanoparticles, and W is the atomic weight of iridium (192.22 g/mol).[72] This calculation yields $Ir_{\sim 150}$ for an average diameter of ∼1.5 nm.

REFERENCES

(1) Aiken, J. D.; Finke, R. G. A review of modern transition-metal nanoclusters: their synthesis, characterization, and applications in catalysis. *J. Mol. Catal. A: Chem.* **1999**, *145*, 1−44.

(2) Crooks, R. M.; Zhao, M.; Sun, L.; Chechik, V.; Yeung, L. K. Dendrimer-Encapsulated Metal Nanoparticles: Synthesis, Characterization, and Applications to Catalysis. *Acc. Chem. Res.* **2001**, *34*, 181−190.

(3) Roucoux, A.; Schulz, J.; Patin, H. Reduced Transition Metal Colloids: A Novel Family of Reusable Catalysts? *Chem. Rev.* **2002**, *102*, 3757−3778.

(4) Astruc, D.; Lu, F.; Aranzaes, J. R. Nanoparticles as Recyclable Catalysts: The Frontier between Homogeneous and Heterogeneous Catalysis. *Angew. Chem., Int. Ed.* **2005**, *44*, 7852−7872.

(5) Chen, T.; Rodionov, V. O. Controllable Catalysis with Nanoparticles: Bimetallic Alloy Systems and Surface Adsorbates. *ACS Catal.* **2016**, *6*, 4025−4033.

(6) Ott, L. S.; Finke, R. G. Transition-metal nanocluster stabilization for catalysis: A critical review of ranking methods and putative stabilizers. *Coord. Chem. Rev.* **2007**, *251*, 1075−1100.

(7) Shen, J.; Ziaei-Azad, H.; Semagina, N. Is it always necessary to remove a metal nanoparticle stabilizer before catalysis? *J. Mol. Catal. A: Chem.* **2014**, *391*, 36−40.

(8) Ott, L. S.; Hornstein, B. J.; Finke, R. G. A Test of the Transition-Metal Nanocluster Formation and Stabilization Ability of the Most Common Polymeric Stabilizer, Poly(vinylpyrrolidone), as Well as Four Other Polymeric Protectants. *Langmuir* **2006**, *22*, 9357−9367.

(9) Smith, J. G.; Jain, P. K. The Ligand Shell as an Energy Barrier in Surface Reactions on Transition Metal Nanoparticles. *J. Am. Chem. Soc.* **2016**, *138*, 6765−6773.

(10) Ahmadi, T. S.; Wang, Z. L.; Green, T. C.; Henglein, A.; El-Sayed, M. A. Shape-Controlled Synthesis of Colloidal Platinum Nanoparticles. *Science* **1996**, *272*, 1924−1926.

(11) Burda, C.; Chen, X.; Narayanan, R.; El-Sayed, M. A. Chemistry and Properties of Nanocrystals of Different Shapes. *Chem. Rev.* **2005**, *105*, 1025−1102.

(12) Tao, A. R.; Habas, S.; Yang, P. Shape control of colloidal metal nanocrystals. *Small* **2008**, *4*, 310−325.

(13) Somorjai, G. A.; Park, J. Y. Colloid Science of Metal Nanoparticle Catalysts in 2D and 3D Structures. Challenges of Nucleation, Growth, Composition, Particle Shape, Size Control and Their Influence on Activity and Selectivity. *Top. Catal.* **2008**, *49*, 126−135.

(14) Aiken, J. D.; Finke, R. G.; Lin, Y. A perspective on nanocluster catalysis: polyoxoanion and $(n\text{-}C_4H_9)_4N^+$ stabilized $Ir(0)_{\sim 300}$ nanocluster 'soluble heterogeneous catalysts'. *J. Mol. Catal. A: Chem.* **1996**, *114*, 29−51.

(15) Campelo, J. M.; Luna, D.; Luque, R.; Marinas, J. M.; Romero, A. A. Sustainable preparation of supported metal nanoparticles and their applications in catalysis. *ChemSusChem* **2009**, *2*, 18−45.

(16) Einaga, H.; Harada, M. Photochemical Preparation of Poly(N-vinyl-2-pyrrolidone)-Stabilized Platinum Colloids and Their Deposition on Titanium Dioxide. *Langmuir* **2005**, *21*, 2578−2584.

(17) Rioux, R. M.; Song, H.; Hoefelmeyer, J. D.; Yang, P.; Somorjai, G. A. High-Surface-Area Catalyst Design: Synthesis, Characterization, and Reaction Studies of Platinum Nanoparticles in Mesoporous SBA-15 Silica. *J. Phys. Chem. B* **2005**, *109*, 2192−2202.

(18) Song, H.; Rioux, R. M.; Hoefelmeyer, J. D.; Komor, R.; Niesz, K.; Grass, M.; Yang, P.; Somorjai, G. A. Hydrothermal Growth of Mesoporous SBA-15 Silica in the Presence of PVP-Stabilized Pt Nanoparticles: Synthesis, Characterization, and Catalytic Properties. *J. Am. Chem. Soc.* **2006**, *128*, 3027−3037.

(19) Rioux, R. M.; Hsu, B. B.; Grass, M. E.; Song, H.; Somorjai, G. A. Influence of Particle Size on Reaction Selectivity in Cyclohexene Hydrogenation and Dehydrogenation over Silica-Supported Monodisperse Pt Particles. *Catal. Lett.* **2008**, *126*, 10−19.

(20) Borodko, Y.; Jones, L.; Lee, H.; Frei, H.; Somorjai, G. A. Spectroscopic Study of Tetradecyltrimethylammonium Bromide Pt−C14TAB Nanoparticles: Structure and Stability. *Langmuir* **2009**, *25*, 6665−6671.

(21) Pang, S.; Kurosawa, Y.; Kondo, T.; Kawai, T. Decomposition of Monolayer Coverage on Gold Nanoparticles by UV/ozone Treatment. *Chem. Lett.* **2005**, *34*, 544−545.

(22) Chen, W.; Kim, J.; Sun, S.; Chen, S. Electro-oxidation of formic acid catalyzed by FePt nanoparticles. *Phys. Chem. Chem. Phys.* **2006**, *8*, 2779−2786.

(23) Park, J. Y.; Aliaga, C.; Renzas, J. R.; Lee, H.; Somorjai, G. A. The Role of Organic Capping Layers of Platinum Nanoparticles in Catalytic Activity of CO Oxidation. *Catal. Lett.* **2009**, *129*, 1−6.

(24) Aliaga, C.; Park, J. Y.; Yamada, Y.; Lee, H. S.; Tsung, C.-H.; Yang, P.; Somorjai, G. A. Sum Frequency Generation and Catalytic Reaction Studies of the Removal of Organic Capping Agents from Pt Nanoparticles by UV−Ozone Treatment. *J. Phys. Chem. C* **2009**, *113*, 6150−6155.

(25) Kim, S.; Qadir, K.; Jin, S.; Satyanarayana, R. A.; Seo, B.; Mun, B. S.; Joo, S. H.; Park, J. Y. Trend of catalytic activity of CO oxidation on Rh and Ru nanoparticles: Role of surface oxide. *Catal. Today* **2012**, *185*, 131−137.

DOI: 10.1021/acsomega.8b01569
ACS Omega 2018, 3, 14538−14550

(26) Eppler, A. S.; Zhu, J.; Anderson, E. A.; Somorjai, G. A. Model catalysts fabricated by electron beam lithography: AFM and TPD surface studies and hydrogenation/dehydrogenation of cyclohexene + H2 on a Pt nanoparticle array supported by silica. *Top. Catal.* **2000**, *13*, 33−41.
(27) Sanchez, S. I.; Small, M. W.; Bozin, E. S.; Wen, J.-G.; Zuo, J.-M.; Nuzzo, R. G. *ACS Nano* **2013**, *7*, 1542−1557.
(28) Bell, A. T. The Impact of Nanoscience on Heterogeneous Catalysis. *Science* **2003**, *299*, 1688−1691.
(29) Johnson, B. F. G. From clusters to nanoparticles and catalysis. *Coord. Chem. Rev.* **1999**, *190−192*, 1269−1285.
(30) Bhattacharya, R.; Mukherjee, P. Biological properties of "naked" metal nanoparticles. *Adv. Drug Delivery Rev.* **2008**, *60*, 1289−1306.
(31) Pagano, R.; Quarta, A.; Pal, S.; Licciulli, A.; Valli, L.; Bettini, S. Enhanced Solar-Driven Applications of ZnO@Ag Patchy Nanoparticles. *J. Phys. Chem. C* **2017**, *121*, 27199−27206.
(32) Ghosh, A.; Bodiuzzaman, M.; Nag, A.; Jash, M.; Baksi, A.; Pradeep, T. Sequential Dihydrogen Desorption from Hydride-Protected Atomically Precise Silver Clusters and the Formation of Naked Clusters in the Gas Phase. *ACS Nano* **2017**, *11*, 11145−11151.
(33) Han, T.; Liu, L. L.; Wei, M. Y.; Wang, C.; Wu, X. Y.; Xie, Z. Q.; Ma, Y. G. Light-activated electric bistability for evaporated silver nanoparticles in organic field-effect transistors. *Phys. Chem. Chem. Phys.* **2017**, *19*, 17653−17660.
(34) Bolzan, G. R.; Abarca, G.; Goncalves, W. D. G.; Matos, C. F.; Santos, M. J. L.; Dupont, J. Imprinted Naked Pt Nanoparticles on N-Doped Carbon Supports: A Synergistic Effect between Catalyst and Support. *Chem. − Eur. J.* **2018**, *24*, 1365−1372.
(35) Zhang, B.; Xue, Y.; Sun, H.; Jiang, A.; Li, Z.; Hao, J. A green synthesis of "naked" Pt and PtPd catalysts for highly efficient methanol electrooxidation. *RSC Adv.* **2016**, *6*, 56083−56090.
(36) Liu, B.; Liu, J. Accelerating peroxidase mimicking nanozymes using DNA. *Nanoscale* **2015**, *7*, 13831−13835.
(37) Lee, T.-L.; Raitano, J. M.; Rennert, O. M.; Chan, S.-W.; Chan, W.-Y. Accessing the genomic effects of naked nanoceria in murine neuronal cells. *Nanomedicine* **2012**, *8*, 599−608.
(38) Ott, L. S.; Finke, R. G. Nanocluster Formation and Stabilization Fundamental Studies: Investigating "Solvent-Only" Stabilization En Route to Discovering Stabilization by the Traditionally Weakly Coordinating Anion BF_4^- Plus High Dielectric Constant Solvents. *Inorg. Chem.* **2006**, *45*, 8382−8393.
(39) Yang, G. K.; Peters, K. S.; Vaida, V. Strength of the metal-ligand bond in $LCr(CO)_5$ measured by photoacoustic calorimetry. *Chem. Phys. Lett.* **1986**, *125*, 566−568.
(40) Simon, J. D.; Xie, X. Photodissociation of chromium hexacarbonyl in 1-propanol and 2-propanol: effect of solvent structure on the mechanisms of formation of $Cr(CO)_5(OHR)$ from photogenerated $Cr(CO)_5(ROH)$. *J. Phys. Chem.* **1989**, *93*, 291−293.
(41) Morse, J. M.; Parker, G. H.; Burkey, T. J. Enthalpy of carbonyl dissociation from metal hexacarbonyls $M(CO)_6$ (M = chromium, molybdenum, tungsten) in alkane solvent: determination of intermolecular agostic bond strengths. *Organometallics* **1989**, *8*, 2471−2474.
(42) He, B.; Chen, Y.; Liu, H.; Liu, Y. J. Synthesis of Solvent-Stabilized Colloidal Nanoparticles of Platinum, Rhodium, and Ruthenium by Microwave-Polyol Process. *J. Nanosci. Nanotechnol.* **2005**, *5*, 266−270.
(43) Vidoni, O.; Philippot, K.; Amiens, C.; Chaudret, B.; Balmes, O.; Malm, J. O.; Bovin, J. O.; Senocq, F.; Casanove, M. J. Novel, spongelike ruthenium particles of controllable size stabilized only by organic solvents. *Angew. Chem., Int. Ed.* **1999**, *38*, 6736−6738.
(44) Curtis, A. C.; Duff, D. G.; Edwards, P. P.; Jefferson, D. A.; Johnson, B. F. G.; Kirkland, A. I.; Wallace, A. S. Preparation and structural characterization of an unprotected copper sol. *J. Phys. Chem.* **1988**, *92*, 2270−2275.
(45) Pelzer, K.; Vidoni, O.; Philippot, K.; Chaudret, B.; Colliere, V. Organometallic Synthesis of Size-Controlled Polycrystalline Ruthenium Nanoparticles in the Presence of Alcohols. *Adv. Funct. Mater.* **2003**, *13*, 118−126.
(46) Esumi, K.; Tano, T.; Meguro, K. Preparation of organo palladium particles from thermal decomposition of its organic complex in organic solvents. *Langmuir* **1989**, *5*, 268−270.
(47) Bayram, E.; Zahmakiran, M.; Ozkar, S.; Finke, R. G. In Situ Formed "Weakly Ligated/Labile Ligand" Iridium(0) Nanoparticles and Aggregates as Catalysts for the Complete Hydrogenation of Neat Benzene at Room Temperature and Mild Pressures. *Langmuir* **2010**, *26*, 12455−12464.
(48) Corey, E. J. General methods for the construction of complex molecules. *Pure Appl. Chem.* **1967**, *14*, 30−37.
(49) Mozaffari, S.; Li, W.; Thompson, C.; Ivanov, S.; Seifert, S.; Lee, B.; Kovarik, L.; Karim, A. M. Colloidal nanoparticle size control: experimental and kinetic modeling investigation of the ligand−metal binding role in controlling the nucleation and growth kinetics. *Nanoscale* **2017**, *9*, 13772−13785.
(50) Peter, M.; Camacho, J. M. F.; Adamovski, S.; Ono, L. K.; Dostert, K. H.; O'Brien, C. P.; Cuenya, B. R.; Schauermann, S.; Freund, H. J. Trends in the Binding Strength of Surface Species on Nanoparticles: How Does the Adsorption Energy Scale with the Particle Size? *Angew. Chem., Int. Ed.* **2013**, *52*, 5175−5179.
(51) Abellan, P.; Parent, L. R.; Al Hasan, N.; Park, C.; Arslan, I.; Karim, A. M.; Evans, J. E.; Browning, N. D. Gaining Control over Radiolytic Synthesis of Uniform Sub-3-nanometer Palladium Nanoparticles: Use of Aromatic Liquids in the Electron Microscope. *Langmuir* **2016**, *32*, 1468−1477.
(52) Taylor, M. G.; Mpourmpakis, G. Thermodynamic stability of ligand-protected metal nanoclusters. *Nat. Commun.* **2017**, *8*, No. 15988.
(53) Fischer, K.; Jonas, K.; Mollbach, A.; Wilke, G. 1. The catalytic conversion of olefins, VIII. Naked nickel as a catalyst for the transalkylation of aluminum trialkyls with α-olefins. *Z. Naturforsch., B: Anorg. Chem., Org. Chem.* **1984**, *39B*, 1011−1021.
(54) Green, M.; Kuc, T. A.; Tayler, S. H. Cationic Transition-metal Complexes. Part I. Synthesis and Reactions of BIs(diene)-rhodium and −iridium Tetrafluoroborates. *J. Chem. Soc. A* **1971**, 2334−2337.
(55) Schrock, R. R.; Osborn, J. A. Coordinatively Unsaturated Cationic Complexes of Rhodium(I), Iridium(I), Palladium(II), and Platinum(II). Generation, Synthetic Utility, and Some Catalytic Studies. *J. Am. Chem. Soc.* **1971**, *93*, 3089−3091.
(56) Hathaway, B. J.; Holah, D. G.; Underhill, A. E. Preparation and properties of some bivalent transition metal tetrafluoroborate-methyl cyanide complexes. *J. Chem. Soc.* **1962**, 2444−2448.
(57) Collman, J. P.; Hegedus, L. S.; Norton, J. R.; Finke, R. G. *Principles and Applications of Organotransition Metal Chemistry*; University Science Books: Mill Valley, CA, 1987.
(58) Hartwig, J. *Organotransition Metal Chemistry. From Bonding to Catalysis*; University Science Books: Sausalito, CA, 2010.
(59) Özkar, S.; Finke, R. G. Iridium(0) Nanocluster, Acid-Assisted Catalysis of Neat Acetone Hydrogenation at Room Temperature: Exceptional Activity, Catalyst Lifetime, and Selectivity at Complete Conversion. *J. Am. Chem. Soc.* **2005**, *127*, 4800−4808.
(60) Watzky, M. A.; Finke, R. G. Transition Metal Nanocluster Formation Kinetic and Mechanistic Studies. A New Mechanism When Hydrogen Is the Reductant: Slow, Continuous Nucleation and Fast Autocatalytic Surface Growth. *J. Am. Chem. Soc.* **1997**, *119*, 10382−10400.
(61) Widegren, J. A.; Aiken, J. D., III; Özkar, S.; Finke, R. G. Additional Investigations of a New Kinetic Method To Follow Transition-Metal Nanocluster Formation, Including the Discovery of Heterolytic Hydrogen Activation in Nanocluster Nucleation Reactions. *Chem. Mater.* **2001**, *13*, 312−324.
(62) Brzezinski, B.; Glowiak, T.; Grech, E.; Malarski, Z.; Sobczyk, L. 1,8-bis(dimethylaminomethyl)naphthalene - a new proton sponge. *J. Chem. Soc., Perkin Trans. 2* **1991**, 1643−1647.
(63) Aiken, J. D.; Finke, R. G. Nanocluster formation synthetic, kinetic, and mechanistic studies. The detection of, and then methods to avoid, hydrogen mass-transfer limitations in the synthesis of

DOI: 10.1021/acsomega.8b01569
ACS Omega 2018, 3, 14538−14550

polyoxoanion- and tetrabutylammonium-stabilized, near-monodisperse 40 +/− 6 angstrom Rh(0) nanoclusters. *J. Am. Chem. Soc.* **1998**, *120*, 9545−9554.
(64) Van Tiep, L.; Bureautardy, M.; Bugli, G.; Djega-Mariadassou, G.; Che, M.; Bond, G. C. The effect of reduction conditions on the chloride content of $IrTiO_2$ catalysts and their activity for benzene hydrogenation. *J. Catal.* **1986**, *99*, 449−460.
(65) Somorjai, G. A.; Park, J. Y. Molecular surface chemistry by metal single crystals and nanoparticles from vacuum to high pressure. *Chem. Soc. Rev.* **2008**, *37*, 2155−2162.
(66) Tsuji, M.; Matsumoto, K.; Jiang, P.; Matsuo, R.; Tang, X.-L.; Nor Kamarudin, K. S. Roles of Pt seeds and chloride anions in the preparation of silver nanorods and nanowires by microwave-polyol method. *Colloids Surf., A* **2008**, *316*, 266−277.
(67) Oh, H.-S.; Yang, J. H.; Costello, C. K.; Wang, Y. M.; Bare, S. R.; Kung, H. H.; Kung, M. C. Selective Catalytic Oxidation of CO: Effect of Chloride on Supported Au Catalysts. *J. Catal.* **2002**, *210*, 375−386.
(68) Steinmetz, W. E. A CoMFA Model of steric and electronic effects of phosphorous ligands. *Quant. Struct.−Act. Relat.* **1996**, *15*, 1−6.
(69) González-Gálvez, D.; Nolis, P.; Philippot, K.; Chaudret, B.; van Leeuwen, P. W. N. M. Phosphine-Stabilized Ruthenium Nanoparticles: The Effect of the Nature of the Ligand in Catalysis. *ACS Catal.* **2012**, *2*, 317−321.
(70) Pan, C.; Katrin, P.; Philippot, K.; Chaudret, B.; Dassenoy, F.; Lecante, P.; Casanove, M. J. Ligand-Stabilized Ruthenium Nanoparticles: Synthesis, Organization, and Dynamics. *J. Am. Chem. Soc.* **2001**, *123*, 7584−7593.
(71) Dassenoy, F.; Philippot, K.; Ould-Ely, T.; Amiens, C.; Lecante, P.; Snoeck, E.; Mosset, A.; Casanove, M. J.; Chaudret, B. Platinum nanoparticles stabilized by CO and octanethiol ligands or polymers: FT-IR, NMR, HREM and WAXS studies. *New J. Chem.* **1998**, *22*, 703−712.
(72) Lide, D. R., Frederikse, H. P. R., Eds. *CRC Handbook of Chemistry and Physics*, 77th ed.; CRC Press: Boca Raton, FL, 1996.
(73) Lin, Y.; Finke, R. G. A More General Approach to Distinguishing 'Homogeneous' from 'Heterogeneous' Catalysis: Discovery of Polyoxoanion and Bu_4N^+-Stabilized, Isolable and Redissolvable, High Reactivity $Ir_{\sim 190\text{-}450}$ Nanocluster Catalysts. *Inorg. Chem.* **1994**, *33*, 4891−4910.
(74) Hornstein, B. J.; Aiken, J. D., III; Finke, R. G. Nanoclusters in Catalysis: A Comparison of CS_2 Catalyst Poisoning of Polyoxoanion- and Tetrabutylammonium-Stabilized 40 ± 6 Å Rh(0) Nanoclusters to 5% Rh/Al_2O_3, Including an Analysis of the Literature Related to the CS_2 to Metal Stoichiometry Issue. *Inorg. Chem.* **2002**, *41*, 1625.
(75) Bayram, E.; Finke, R. G. Quantitative 1,10-Phenanthroline Catalyst-Poisoning Kinetic Studies of $Rh(0)_n$ Nanoparticle and Rh_4 Cluster Benzene Hydrogenation Catalysts: Estimates of the Poison $K_{association}$ Binding Constants, of the Equivalents of Poison Bound and of the Number of Catalytically Active Sites for Each Catalyst. *ACS Catal.* **2012**, *2*, 1967−1975.
(76) De Jong, K. P.; Geus, J. W. Production of supported silver catalysts by liquid-phase reduction. *Appl. Catal., A* **1982**, *4*, 41−51.
(77) Bond, G. C.; Rawle, A. F. Catalytic hydrogenation in the liquid phase. Part 1. Hydrogenation of isoprene catalysed by palladium, palladium-gold and palladium-silver catalysts. *J. Mol. Catal. A: Chem.* **1996**, *109*, 261−271.
(78) Sales, E. A.; Benhamida, B.; Caizergues, V.; Lagier, J.-P.; Fiévet, F.; Bozon-Verduraz, F. Alumina-supported Pd, Ag and Pd−Ag catalysts: Preparation through the polyol process, characterization and reactivity in hexa-1,5-diene hydrogenation. *Appl. Catal., A* **1998**, *172*, 273−283.
(79) Bonet, F.; Grugeon, S.; Urbina, R. H.; Tekaia-Elhsissen, K.; Tarascon, J.-M. n situ deposition of silver and palladium nanoparticles prepared by the polyol process, and their performance as catalytic converters of automobile exhaust gases. *Solid State Sci.* **2002**, *4*, 665−670.
(80) Zawadzki, M.; Okal, J. Synthesis and structure characterization of Ru nanoparticles stabilized by PVP or γ-Al_2O_3. *Mater. Res. Bull.* **2008**, *43*, 3111−3121.
(81) Boutros, M.; Denicourt-Nowicki, A.; Roucoux, A.; Gengembre, L.; Beaunier, P.; Gédéon, A.; Launay, F. A surfactant-assisted preparation of well dispersed rhodium nanoparticles within the mesopores of AlSBA-15: characterization and use in catalysis. *Chem. Commun.* **2008**, 2920−2922.
(82) Mondloch, J. E.; Finke, R. G. Kinetic Evidence for Bimolecular Nucleation in Supported-Transition-Metal-Nanoparticle Catalyst Formation in Contact with Solution: The Prototype Ir(1,5-COD)-Cl/γ-Al_2O_3 to $Ir(0)_{900}/\gamma$-Al_2O_3 System. *ACS Catal.* **2012**, *2*, 298−305.
(83) Mondloch, J. E.; Wang, Q.; Frenkel, A. I.; Finke, R. G. Development Plus Kinetic and Mechanistic Studies of a Prototype Supported-Nanoparticle Heterogeneous Catalyst Formation System in Contact with Solution: Ir(1,5-COD)Cl/γ-Al_2O_3 and Its Reduction by H_2 to $Ir(0)(n)/\gamma$-Al_2O_3. *J. Am. Chem. Soc.* **2010**, *132*, 9701−9714.
(84) Kent, P.; Mondloch, J. E.; Finke, R. G. Synthesis of Heterogeneous $Ir\sim_{600\text{-}900}/\gamma$-$Al_2O_3$ in One Pot From the Precatalyst Ir(1,5-COD)Cl/γ-Al_2O_3: Discovery of Two Competing Trace "Ethyl Acetate Effects" on the Nucleation Step and Resultant Product. *ACS Catal.* **2016**, *6*, 5449−5461.
(85) Mondloch, J. E.; Finke, R. G. Supported-Nanoparticle Heterogeneous Catalyst Formation in Contact with Solution: Kinetics and Mechanism of the Conversion of Ir(1,5-COD)Cl/γ-Al_2O_3 to $Ir(0)_{\sim 900}/\gamma$-Al_2O_3. *J. Am. Chem. Soc.* **2011**, *133*, 7744−7756.
(86) Mondloch, J. E.; Yan, X.; Finke, R. G. Monitoring Supported-Nanocluster Heterogeneous Catalyst Formation: Product and Kinetic Evidence for a 2-Step, Nucleation and Autocatalytic Growth Mechanism of $Pt(0)_n$ Formation from H_2PtCl_6 on Al_2O_3 or TiO_2. *J. Am. Chem. Soc.* **2009**, *131*, 6389−6396.
(87) Zheng, N.; Stucky, G. D. A General Synthetic Strategy for Oxide-Supported Metal Nanoparticle Catalysts. *J. Am. Chem. Soc.* **2006**, *128*, 14278−14280.
(88) Boualleg, M.; Basset, J.-M.; Candy, J.-P.; Delichere, P.; Pelzer, K.; Veyre, L.; Thieuleux, C. Regularly distributed and fully accessible Pt nanoparticles in silica pore channels via the controlled growth of a mesostructured matrix around Pt colloids. *Chem. Mater.* **2009**, *21*, 775−777.
(89) Watzky, M. A.; Finney, E. E.; Finke, R. G. Transition-Metal Nanocluster Size vs Formation Time and the Catalytically Effective Nucleus Number: A Mechanism-Based Treatment. *J. Am. Chem. Soc.* **2008**, *130*, 11959−11969.
(90) Fonseca, G. S.; Scholten, J. D.; Dupont, J. Iridium nanoparticles prepared in ionic liquids: An efficient catalytic system for the hydrogenation of ketones. *Synlett* **2004**, *9*, 1525−1528.
(91) Dupont, J.; Fonseca, G. S.; Umpierre, A. P.; Fichtner, P. F. P.; Teixeira, S. R. Transition-Metal Nanoparticles in Imidazolium Ionic Liquids: Recycable Catalysts for Biphasic Hydrogenation Reactions. *J. Am. Chem. Soc.* **2002**, *124*, 4228−4229.
(92) Dupont, J.; Meneghetti, M. R. On the stabilisation and surface properties of soluble transition-metal nanoparticles in non-functionalised imidazolium-based ionic liquids. *Curr. Opin. Colloid Interface Sci.* **2013**, *18*, 54−60.
(93) Scholten, J. D.; Leal, B. C.; Dupont, J. Transition Metal Nanoparticle Catalysis in Ionic Liquids. *ACS Catal.* **2012**, *2*, 184−200.
(94) Migowski, P.; Zanchet, D.; Machado, G.; Gelesky, M. A.; Teixeira, S. R.; Dupont, J. Nanostructures in ionic liquids: correlation of iridium nanoparticles' size and shape with imidazolium salts' structural organization and catalytic properties. *Phys. Chem. Chem. Phys.* **2010**, *12*, 6826−6833.
(95) Lei, X.; Yang, L.; Zhang, F.; Duan, X. A novel gas−liquid contacting route for the synthesis of layered double hydroxides by decomposition of ammonium carbonate. *Chem. Eng. Sci.* **2006**, *61*, 2730−2735.
(96) Muehling, J. K.; Arnold, H. R.; House, J. E., Jr. Effects of particle size on the decomposition of ammonium carbonate. *Thermochim. Acta.* **1995**, *255*, 347−353.

DOI: 10.1021/acsomega.8b01569
ACS Omega 2018, 3, 14538−14550

(97) Woehrle, G. H.; Hutchison, J. E.; Özkar, S.; Finke, R. G. Analysis of Nanoparticle transmission Electron Microscopy Data Using a Public Domain Image-processing Program, Image. *Turk. J. Chem.* **2006**, *30*, 1−13, DOI: 10.3906/kim-0508-1.

DOI: 10.1021/acsomega.8b01569
ACS Omega 2018, 3, 14538−14550